Thermal Model of an Omnimagnet for Performance Assessment and Temperature Control

Fateme Esmailie
Department of Mechanical Engineering,
University of Utah,
Salt Lake City, UT 84112
e-mail: ameel@mech.utah.edu

Matthew S. Cavilla
Department of Mechanical Engineering,
University of Utah,
Salt Lake City, UT 84112
e-mail: Matt.cavilla@utah.edu

Jake J. Abbott
Professor
Department of Mechanical Engineering,
University of Utah,
Salt Lake City, UT 84112
e-mail: jake.abbott@utah.edu

Tim A. Ameel[1]
Professor
Department of Mechanical Engineering,
University of Utah,
Salt Lake City, UT 84112
e-mail: ameel@mech.utah.edu

An Omnimagnet is an electromagnetic device that enables remote magnetic manipulation of devices such as medical implants and microrobots. It is composed of three orthogonal nested solenoids with a ferromagnetic core at the center. Electrical current within the solenoids leads to undesired temperature increase within the Omnimagnet. If the temperature exceeds the melting point of the wire insulation, device failure may occur. Thus, a study of heat transfer within an Omnimagnet is a necessity, particularly to maximize the performance of the device. A transient heat transfer model that incorporates all three heat transfer modes is proposed and experimentally validated with an average normalized root-mean-square error of less than 4% (data normalized by temperature in degree celsius). The transient model is not computationally expensive and is applicable to Omnimagnets with different structures. The code is applied to calculate the maximum safe operational time at a fixed input current or the maximum safe input current for a fixed time interval. The maximum safe operational time and maximum safe input current depend on size and structure of the Omnimagnet and the lowest critical temperature of all the Omnimagnet materials. A parametric study shows that increasing convective heat transfer during cooling, and during heating with low input currents, is an effective method to increase the maximum operational time of the Omnimagnet. The thermal model is also presented in a state-space equation format that can be used in a real-time Kalman filter current controller to avoid device failure due to excessive heating. [DOI: 10.1115/1.4049869]

Keywords: transient, lumped capacitance, state-space, thermal management, Omnimagnet, optimization

Introduction

An Omnimagnet [1] is a relatively new electromagnetic device that enables remote magnetic manipulation [2] of devices such as medical implants and microrobots. We are particularly interested in its use for robotically assisted insertion of cochlear-implant electrode arrays [3–5], in which an Omnimagnet is adjacent to the patient's head during surgery. An Omnimagnet is composed of three orthogonal nested solenoids with a spherical ferromagnetic core at the center and is optimized to generate a dipole-like magnetic field in any direction. By independently controlling the input current to the three solenoids, the magnitude and direction of the resulting dipole moment can be managed. The Omnimagnet magnetic field is capable of applying both force and torque in a desired direction and magnitude to precisely manipulate medical implants, thus enabling insertion. The electrical current flowing through the solenoids produces Joule heating, which results in undesirable temperature increase within the Omnimagnet. If the temperature of the wire insulation exceeds its critical temperature in any of the solenoids, a short circuit may occur, resulting in irreversible device failure. Thus, a heat transfer study is necessary to define operational limits for the Omnimagnet. Additionally, a heat transfer model can be employed to improve future designs of Omnimagnets.

Petruska and Abbott [1] briefly considered heat transfer in an Omnimagnet as a part of the original design process. They assumed a steady-state condition and calculated the maximum current density for a desired magnetic field strength. Transient heat transfer within the Omnimagnet has not been previously studied. Other relevant research is related to heat-transfer studies within power transformers. The heat source in both a power transformer and an Omnimagnet is resistive heating, and the materials (copper, electrically resistive paper, and polyamide insulation) are similar. Thus, the basic heat transfer within a power transformer and an Omnimagnet is alike; hence, the published work on power-transformer heat transfer is relevant. Temperature is a key factor in controlling power transformer aging. Based on the international standards for oil-immersed transformers (IEC 60076–7), the aging rate of power transformers is normal at temperatures lower than 98 °C. For every 6 °C temperature increase, the lifetime of a transformer is reduced by 50% [6]. Another key performance parameter in transformers is hot-spot location. Locating hot spots and calculating their temperature are two of the primary reasons researchers have investigated power-transformer heat transfer [7–9]. Computational fluid dynamics (CFD) and thermal network models (TNM)/thermal hydraulic network models (THNM) are two of the main techniques that have been applied to model heat transfer within power transformers [10–13]. In the review paper by Campelo et al., it was reported that increasing oil flowrate does not significantly change the convection coefficient in high-voltage power transformers [6]. They concluded that CFD and TNM methods produced the most accurate thermal models for power transformers. CFD methods were reported to be more accurate, but computationally expensive, and as a result, researchers are using TNM frequently in their studies [10].

[1]Corresponding author.

A Preliminary Version of this Work was Presented At IMECE 2017: Paper Number IMECE2017-72120.

Contributed by of ASME for publication in the Journal of Thermal Science and Engineering Applications. Manuscript received September 4, 2020; final manuscript received January 5, 2021; published online March 10, 2021. Assoc. Editor: Prabal Talukdar.

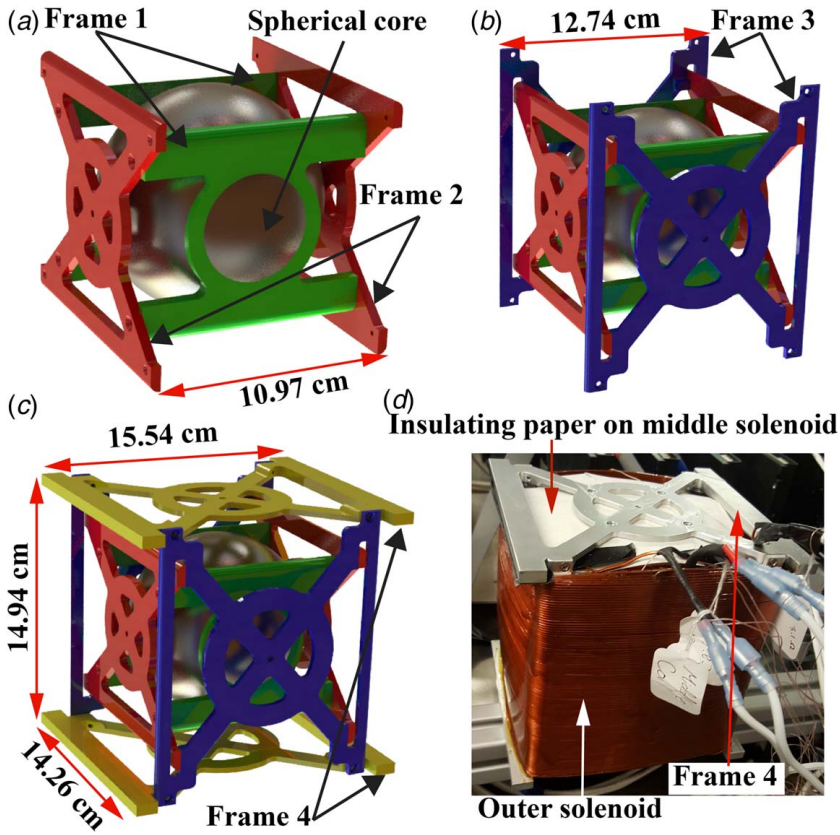

Fig. 1 Omnimagnet components. (*a*) Frame 1, Frame 2, and the spherical core; (*b*) Frame 3 is added; (*c*) Frame 4 is added. The three solenoids, which are wound around the respective frames, are omitted for clarity. The dimensions shown are for one particular Omnimagnet design, but the device can be scaled homothetically. (*d*) Photo of an assembled Omnimagnet.

Research studies focused on modeling heat transfer within power transformers are still being reported [9,14]. For instance, Rodriguez et al. [12] focused on the cooling capacity of radiators that have been used to decrease the temperature of the windings. They performed experiments to validate their simulation results and showed that oil is 10 times more efficient than air in cooling the transformer. They also reported that the air flowrate has only a minor effect on convective cooling of the transformer.

In most heat-transfer studies related to power transformers, a steady-state condition has been applied. Power transformers typically operate continuously at steady-state; thus, the spatial temperature distribution has been the main objective of most studies. On the contrary, an Omnimagnet is typically activated for a relatively short period of time and does not reach a steady-state condition; therefore, the transient temperature response is more desirable.

Probably, the most important outcome in an Omnimagnet heat-transfer study is the maximum time the device can be operated, for a given power distribution in the three coils, before its failure. Alternatively, one is interested in the maximum power that can be applied for a certain period of time. Therefore, a steady-state assumption is inappropriate for an analysis of Omnimagnet thermal behavior.

Methods to mitigate temperature rise in electrical devices such as power transformers have also been pursued recently. For instance, modified nanomaterials with better thermal properties (higher thermal conductivity and higher cooling convection coefficient) [15–17] and magnetic fluid coolants [18,19] are two interesting adaptations that have been studied. Mineral oil has been used as a cooling fluid in transformers. Nanofluids have also been used as alternative coolants. The thermal conductivity of nanofluids can be as much as 75% greater than that for mineral oil, making these new substances attractive as coolants. Increasing the operational temperature limit for wire insulation is also an attractive upgrade for transformers. Typical wire insulation consists of polyamide. New nanomaterials (aliphatic polyamide) that are reinforced with SiO_2, Al_2O_3, and TiO_2 have been patented by Weinberg and Senyurt [20]. These alternative insulations have better thermal properties than pure polyamide. In addition, carbon nanotube (CNT) materials can potentially replace copper wire, as they have high thermal and electrical conductivity [15,21]. As a method to increase transformer cooling rate, Patel et al. have used a magnetic fluid as a coolant. A Mn-Zn ferrite magnetic fluid (TCF-56) can reduce the winding, core, and top oil temperatures by 20°C, 14°C, and 21°C, respectively [19].

In practice, an Omnimagnet operates for short time intervals, so it is unlikely that a steady-state thermal condition is reached. Thus, calculating the maximum allowable current density (as in Petruska and Abbott [1]) to produce a desired magnetic field does not provide transient temperature data. In this study, a transient thermal model of an Omnimagnet is developed and validated for the first time. A preliminary version of this work was presented in Ref. [22]. The model is applied to determine the relationship between current density and thermal limits. In addition, potential cooling methods are investigated. Finally, a model in state-space form is provided to facilitate control of the magnetic field strength while taking into account transient temperature increase.

Thermal Lumped Capacitance Model

The details of an Omnimagnet design are presented in Ref. [1]. The main components include frames, solenoids (coils), wire insulation, and a ferromagnetic core. The ferromagnetic core can be spherical or cubical. An Omnimagnet may be thermally modeled as a set of its elements (see Fig. 1).

- Frames: Four sets of two identical parallel frames are included (four elements).
- Solenoids: Three solenoids of copper wire wound around each frame are the main components of an Omnimagnet (three elements).
- Wire insulation: Solenoid wires are insulated; however, each solenoid is modeled as a copper solid rather than a conglomeration of separate wires. Thus, the wire insulation is also modeled as a single solid surrounding the solenoid conductor (three elements).
- Ferromagnetic core: A solid ferromagnetic spherical or cubical core is located in the middle of the Omnimagnet to magnify the electromagnetic field; this sphere/cube is considered a separate element (one element).

In addition to the main components, the design may include extra electrical insulation to ensure the safety of the Omnimagnet. These insulation layers are modeled as separate components.

- Cover insulation: The outer surface of each solenoid is covered with an additional layer of thin electrically resistive insulation (three elements).
- Insulating paper or Kapton tape: Thermal insulating paper or Kapton tape is placed between each solenoid and the surrounding frames.
- Material in the innermost region: The material that fills the deepest part of the Omnimagnet is modeled as an independent element. This gap may be filled with trapped air or any other material.

The four frames, each consisting of two parallel frame sections, and their assembly for a sample Omnimagnet are shown in Fig. 1. Inner, middle, and outer solenoids are wound around Frame 1, Frame 2, and Frame 3, respectively. Frame 4 is used as a support to join all the parts together. An image of a complete Omnimagnet is shown in Fig. 1(*d*). The wire insulation and outer insulating cover insulation are optically transparent; thus, they are not visible in the photo.

Due to the high-thermal conductivity k of most Omnimagnet components (on the order of 10–100 (W/m · K)), low convection coefficient h (natural convection assumed, $0-25$ (W/m^2 · K)), the small characteristic length L of each component (< 0.2 m), the Biot number Bi for each element is less than 0.1. The Biot number is defined as $Bi = hL/k$, where L is calculated as the ratio of the component volume to its surface area. To be conservative in the estimate of component Bi, h is assumed to be 25 (W/m^2 · K). As an example, the volume and surface area of wire insulation1 are approximately 54.9 cm^3 (see Table 1) and 582 cm^2, respectively; thus, L is approximately 0.094 cm and Bi is approximately 0.094. Using this approach, Bi for components 1 to 16 is 0.0005, 0.0003, 0.0003, 0.0003, 0.002, 0.0002, 0.0002, 0.094, 0.086, 0.08, 0.092, 0.005, 0.086, NA, 0.03, and 0.03, respectively. Owing to the small Bi for each component and symmetry, it is reasonable to model the Omnimagnet using a lumped-capacitance method. The main assumptions for the application of this method to the elements of the Omnimagnet include the following:

- Temperature distribution is uniform in each element ($Bi < 0.1$).
- Conduction between elements is modeled with Fourier's Law, where the differentials are approximated with variable differences.
- Thermal contact resistance is neglected.
- The temperature of the surroundings is equal to that of ambient air.
- All thermal properties of the elements (except the copper coils) are considered to be temperature independent.
- Radiation heat transfer between different elements is neglected; however, radiation between the surrounding and insulating paper, Frame 4, wire insulation of solenoid 3, cover insulation of the solenoid 3, and outer solenoid (solenoid 3) is included.
- Electrical insulating materials (paper or Kapton tape) is placed between each solenoid and the surrounding frames. These insulating layers can be incorporated in the model as correction coefficients.
- The view factor between solenoid 2 and ambient and the view factor between solenoid 3 and ambient are both assumed to be unity.

Utilizing these simplifying assumptions and applying an energy balance to each element, n ordinary differential equations (ODEs) are developed for n unknown temperatures. n is the number of elements of the Omnimagnet. The number of elements includes the principal elements (11 elements), the inside trapped material (one element) and the number of extra electrical insulation layers. The general form of the ODE for each element is

$$\rho_i c_{pi} V_i \frac{dT_i}{dt} = R_i I_i^2 - \left[\sum_{j=1, j\neq i}^{j=n}\left(\sum_{m=1}^{m=3}\kappa_j S_{i,j,m}\frac{T_i - T_j}{\Delta x_{j,m}}\right)\right] - \left[\sum_{j=0|\,j=14}\left(\sum_{m=1}^{m=3} h_{i,j} S_{i,j,m}(T_i - T_j)\right)\right] - \sum_{m=1}^{m=3}\sigma\epsilon_i S_{i,0,m}(T_i^4 - T_0^4) \quad (1)$$

The variables ρ_i, V_i, c_{pi}, T_i, ϵ_i, R_i, and I_i are density (kg/m^3), volume (m^3), specific heat capacity at constant pressure (kJ/kg · K), temperature (K), emissivity, electrical resistance (Ω), and input current (A) of the ith element, respectively. κ_j is thermal conductivity (W/m · K) of the jth element. I_i is nonzero only for the three solenoids. Time (s) is represented by t. $S_{i,j,m}$ and $\Delta x_{j,m}$ are contact surface area (m^2) and thickness (m) between the ith and jth elements in the m direction ($x = 1$, $y = 2$, or $z = 3$), respectively. Note that $S_{i,j,m} = S_{j,i,m}$. $h_{i,j}$ is the convection coefficient (W/m^2 · K) between the ith element and the ambient ($j = 0$) or the inner air ($j = 14$). $h_{i,j}$ is a function of temperature and the orientation of the surface. Based on the orientation of the heated surface $h_{i,j}$ can be estimated by the convection coefficient correlation in an enclosure $(h_{i,j})_{encl}$, over a vertical surface $(h_{i,j})_v$, above a horizontal surface $(h_{i,j})_{ha}$, or below a horizontal surface $(h_{i,j})_{hb}$. All heat transfer coefficient correlations are provided in Appendix A for a specific Omnimagnet.

T_{14} is the temperature of the innermost trapped fluid (K). Note that if the gap inside the inner solenoid (Solenoid 1) and the middle solenoid (Solenoid 2) is filled with a solid, this term is replaced by a conduction term. σ is the Stefan–Boltzmann constant (5.67×10^{-8} (W/m^2 · K^4)) and T_0 is ambient temperature (K) of the air surrounding the device. The term on the left-hand side of Eq. (1) is the storage term for the ith element. The first term on the right-hand side of Eq. (1) represents heat source. Source terms are applicable only to the equations related to the three solenoids. The second term represents conduction between elements, the third term represents convection to the inside trapped fluid, the convection to ambient if the component is exposed to the ambient air, and the fourth term represents radiation exchange with the surroundings. Radiation is included in the equations related to the outer solenoid, the outermost frame (Frame 4), and the insulating paper.

Equation (1) is applied to each of the n elements to produce n ODEs with n unknown element temperatures. The model requires input data such as initial temperature, volume and thickness of each element, contact surface area between two adjacent elements, thermal properties, convection coefficients, and electrical resistance and input current of each solenoid. An example of the thermal model applied to a specific Omnimagnet is presented in Appendix A. The equation set is solved using MATLAB (function ode45). The ode45 function uses the last time-step to provide the results for the next time-step using an explicit Runge–Kutta (4,5) method [23]. A state-space format of the equations is provided in Appendix B. Simulations from the model should be validated and assessed for accuracy by comparisons to experimental data. An

experimental apparatus and test procedure for model validation are presented in the following section.

Experimental Setup

A schematic of the experimental setup is depicted in Fig. 2. An AMC high-frequency PWM servo drive provides an effectively constant electrical input current to the solenoids. Two Omega type-K thermocouples are implanted on opposite sides of each solenoid, near the coil center, to measure temperature. The location of each thermocouple depends on the number of windings in each solenoid. The thermocouples are implanted at the middle layer if there are an even number of layers, and one wire toward the core from that if there is an odd number of layers. Two similar thermocouples are used to measure the ambient air temperature and the air temperature beneath the center of the Omnimagnet. Electrical resistance of each solenoid is measured using a Fluke 87 True-RMS Multimeter at the beginning of each experiment. All temperature data are recorded every 0.5 s, and the electrical potential difference of each solenoid is measured every 5 min.

The computer and AMC servo drive together control the input current and maintain it at the desired value to each solenoid. As temperature increases, the copper wire resistance changes, requiring modifications to the applied voltage to achieve a constant current. The control loop functions between the computer and the solenoids and does not require temperature feedback. In Fig. 2, the line between the data acquisition system (DAQ) and the computer indicates temperature data acquired and stored on the computer.

The critical temperature in the experiment is equivalent to the lowest melting point of all the component materials. For the Omnimagnet used in the experiments, the cover insulation melting point, and thus the critical temperature, is 120 °C. In the absence of the cover insulation, the critical temperature would be equivalent to the melting point of the wire insulation, which is 240 °C. The experiment is stopped when the maximum temperature is 5 °C lower than the critical temperature or after 2 h. The maximum time that the Omnimagnet is powered depends on the input current; higher input current leads to shorter safe operating time. Experimental data from this process are used to validate simulation results as presented in Appendix A.

To validate the model, 40 independent experiments were conducted on the lab-scale Omnimagnet. In each experiment, temperatures of the three solenoids were measured at two separate locations (six measurements total) as a function of time. Measurements were repeated for three current levels and different combinations of powered solenoids (20 heating experiments). Passive Omnimagnet cooling was also considered (20 experiments).

Uncertainty Analysis and Sources of Errors. A single thermocouple from a batch of identical thermocouples was selected as the reference thermocouple. This thermocouple was calibrated using a two-point method, and the uncertainty of the temperature measurement was determined to be 0.1 °C. All thermocouples embedded in the Omnimagnet solenoids were from the same batch of thermocouples as the reference thermocouple. The error range of the multimeter (Fluke 87 True-RMS) is 0.05% of the reading plus one digit for voltage and 0.2% of the reading plus 2 digits for electrical resistance [24]. Using the voltage and resistance uncertainties, the electrical current uncertainty is 0.001 A. Finally, the time measurement uncertainty is 0.5 s [25].

Validation and Optimization

Omnimagnets are manually wound; therefore, some uncertainty exists in values required as input data to the model. For instance, the exact value of the contact surface area between different elements, the thermal contact resistance, and the thickness of the various insulation layers is not easily measurable and is not reported. Given these unknown parameters, the following assumptions are made to the model initially:

- Contact resistance between different elements is neglected.
- Each solenoid is in perfect contact with its frame and with the adjacent solenoid(s). Thus, the maximum contact area between elements is assumed.
- Thickness of all elements is assumed to be constant. Shrinkage or expansion due to winding pressure or temperature increase is neglected.

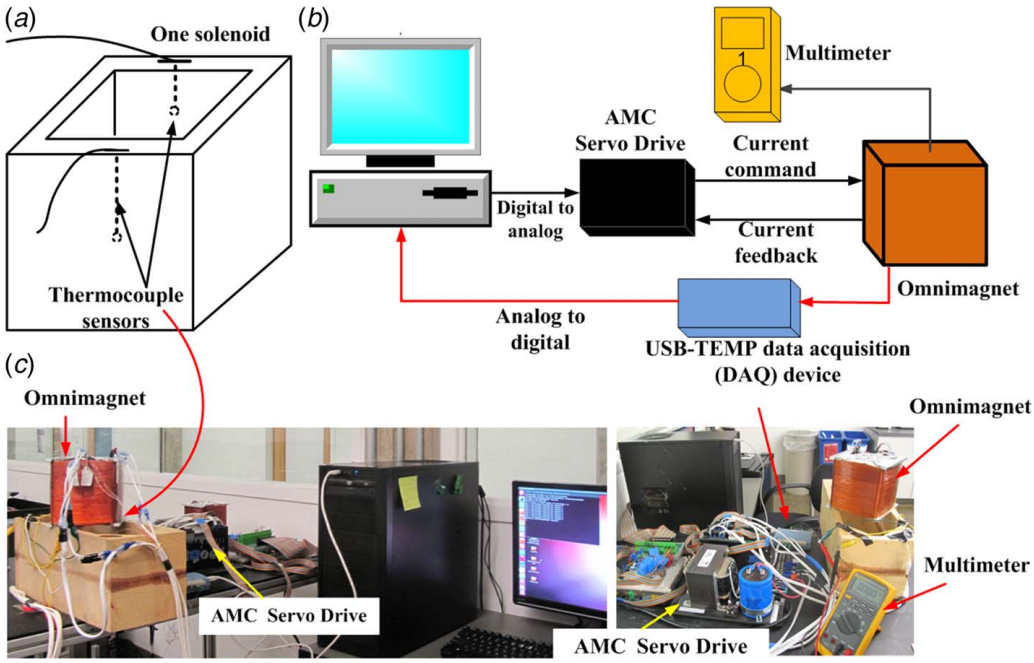

Fig. 2 Experimental setup: (*a*) location of thermocouples in each solenoid, (*b*) schematic, and (*c*) photos

The model is solved applying these assumptions and the resulting temperature data are compared with experimental data. Conditions in the model are set to match those used in the experiments. If the differences between the experiment and simulation temperatures for the solenoids are acceptable, this model can be applied for further studies or for controlling the system. The initial validation process produced an average NRMSE of 26.7% (data are normalized with temperature in degree celsius) with similar transient temperature trends for the three solenoid experimental and model data sets. This error is due to the aforementioned uncertainties; however, better performance can be achieved by modifying the model using experimental data. To reduce the error and to ultimately create a more accurate model, a set of coefficients is added to the basic code. These coefficients are applied to the terms with uncertain dimensions (e.g., thickness, contact area) and where there is a high probability that contact resistance may be present. In addition, some coefficients are used as correction factors in the convection heat transfer terms to better estimate convection coefficients. All assumptions and simplifications presented in the previous paragraph are incorporated through these correction coefficients.

The number of correction coefficients and the appropriate terms to augment in the model depends on the structure of any specific Omnimagnet. As an initial step, a correction coefficient is added to each term and an optimization process is performed. If a correction coefficient is found to be small after optimization, that coefficient can be neglected. Only the correction coefficients that cause a significant change to the final results (minimization of the difference between model and experimental data) in the optimization process are incorporated into the model.

As noted, an optimization process is performed to determine appropriate values for the correction coefficients based on minimization of the solenoid temperature differences between the experiments and simulations. During the optimization process, transient solenoid temperatures for seven experiments corresponding to the seven combinations of powered solenoids are evaluated and compared with simulation data determined under similar conditions. A MATLAB optimization toolbox (using the fmincon "interior point algorithm" [26]) is used to minimize the maximum solenoid temperature difference by varying the coefficients using a quasi-Newton method. The algorithm is illustrated in Fig. 3. The final result is a semi-empirical model, based on the lumped capacitance method, for the Omnimagnet. The coefficients for the conduction terms can vary between 0 and 1. On the other hand, the coefficients for the convection terms can be larger than one, but the upper limit for convection coefficients should not exceed the upper limit for the type of the convection used to cool the Omnimagnet (e.g., for natural convection in air the convection coefficient should not exceed 25 $W/m^2 \cdot K$ [27].

The model is applied to the Omnimagnet used in the experiments. Details of the input data for the Omnimagnet are presented in Appendix A. Following the optimization process, the average normalized root mean square error is less than 4% (data are normalized by temperature in °C) at solenoid temperatures less than 120 °C. Comparisons of simulation and experiment transient temperatures for the three solenoids are shown in Fig. 4. In Fig. 4(*a*), only the inner solenoid (Solenoid 1) is powered (at 3.13 A). The average normalized-root-mean-square error in this case is 2.5%. During cooling, no electrical current is flowing in any part of the system (Fig. 4(*b*)). The model accurately predicts solenoid temperatures under conditions of natural convection and radiation cooling (NRMSE = 2.7%). Transient solenoid temperature response when current is applied to the middle (Solenoid 2) and outer solenoids (Solenoid 3) (3.04 A in each) is shown in Fig. 4(*c*). Note that the average error (NRMSE = 3.7%) is nearly equal to that when only the inner solenoid is powered (NRMSE = 2.5%). Finally, the transient solenoid temperature response when all three solenoids are powered at 3.8 A is presented in Fig. 4(*d*), where the average NRMSE is 2.1%. These errors are deemed acceptable given the uncertainties in some of the input data and the assumptions inherent to the lumped capacitance method. When using an Omnimagnet in practice, a factor of safety can be included that accounts for this level of modeling error.

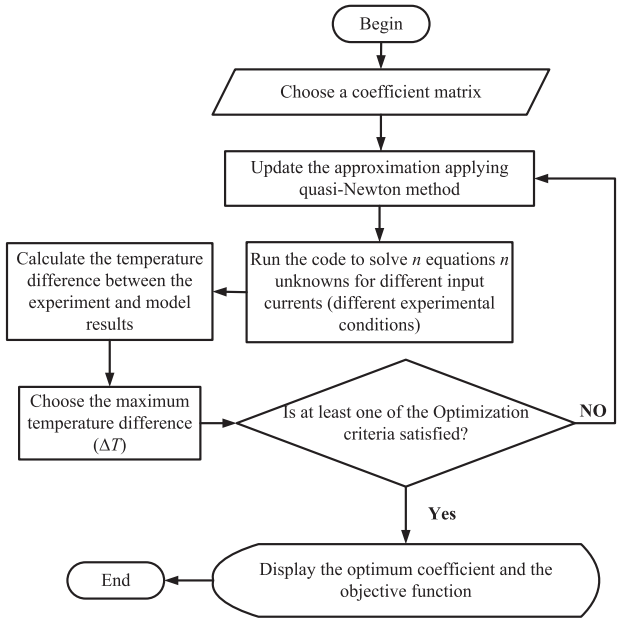

Fig. 3 Optimization algorithm to determine modification coefficients

Results and Discussion

After validation, the model is used to study the thermal behavior of the Omnimagnet under different conditions. Of most interest is the maximum time t_{max}, the Omnimagnet can be powered before the maximum temperature T_{max} in the device reaches the temperature limit (melting point), which for the Omnimagnet prototype (see Appendix A) is 115 °C. t_{max} data are shown in Fig. 5 for seven cases corresponding to seven combinations of solenoids carrying current I.

As shown in Fig. 5, when cooling is achieved by natural convection and radiation with the surroundings, the worst-case scenario occurs when all three solenoids are powered simultaneously. The inner solenoid heats more quickly than the other two, due to the high thermal resistance between the inner solenoid (solenoid 1) and the ambient. According to the data in Fig. 5, free convection is not very effective in removing excess heat from the Omnimagnet, which limits the time the device can be powered. Thus, more effective cooling mechanisms should be considered. Increasing the convection heat transfer coefficient on the surface of the middle and outer coils, which are exposed to the ambient, is an option to decrease T_{max} and subsequently increase t_{max}. The effect of the convection heat transfer coefficient is discussed in the next section.

Effect of *h* for Heating and Cooling. The inner solenoid is not exposed to the ambient; so, it is not directly affected by convective cooling from the outer surfaces of the Omnimagnet. On the other hand, all four external surfaces of the outer solenoid and two of the four external surfaces of the middle solenoid are exposed to convective cooling with ambient air. Therefore, it is expected that increasing the convective heat transfer coefficient will directly affect the transient temperature response of the middle and outer solenoids while the inner solenoid will only be indirectly influenced. The effect of h on the temperature of the solenoids is studied in both cooling and heating modes. A set of four different values of h are selected for the study. A heat transfer coefficient equal to 5 $(W/m^2 \cdot K)$ is chosen as a representation of natural convection in air. A value of 250 $(W/m^2 \cdot K)$ represents forced

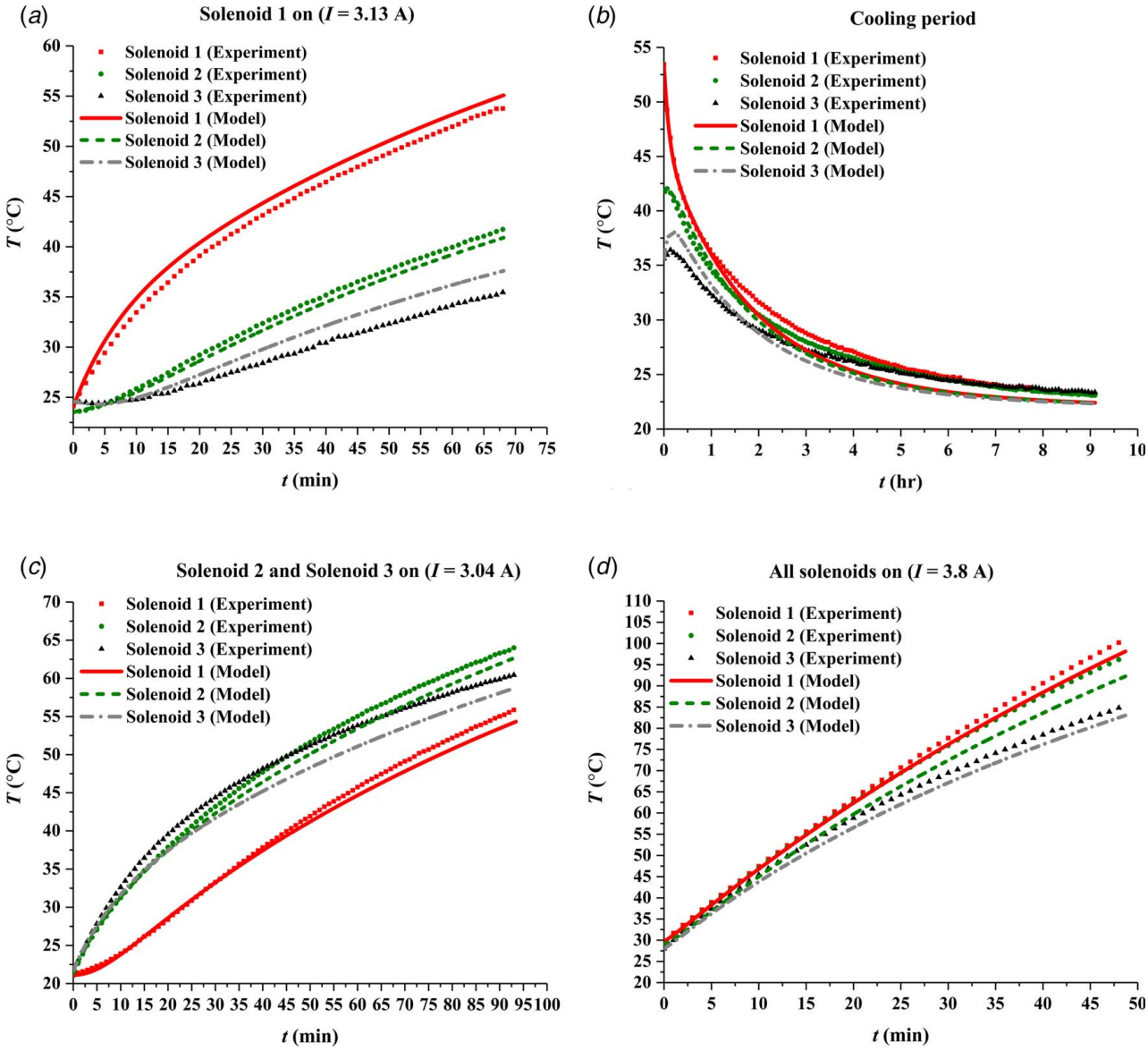

Fig. 4 Experimental validation of the model: (*a*) inner solenoid on, (*b*) cooling period, no current flow, (*c*) middle and outer solenoids on, and (*d*) all three solenoids on

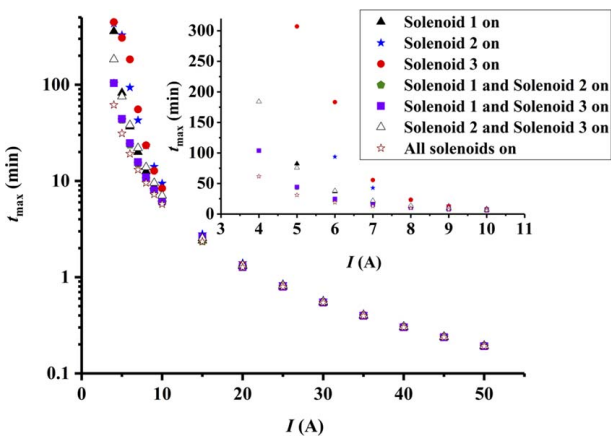

Fig. 5 Maximum operational time for the omnimagnet under seven different combinations of powered solenoids in a range of current from 0 to 50 A and natural-convection cooling

convection in air, and 500 and 1000 (W/m^2·K) correspond to natural convection in a liquid media, which can be produced by nanofluids as mentioned in the Introduction section. The effect of h for six different values of input current applied only to the outer solenoid is shown in Fig. 6. Generally, the heating rate for the solenoid with the highest temperature (Solenoid 3) is slowed as h increases, but this effect is tempered at higher input current. For large I (depending on size and structure of the Omnimagnet), this effect is negligible. At lower current, the input power is of the same order of magnitude as the convection heat transfer rate, which enables control of the Omnimagnet temperature. According to Eq. (1), doubling the current leads to four times the power. As a result, for larger values of I, increases in convection coefficient have less effect on reducing the rate of temperature increase, making a maximum safe operating temperature impossible. It should also be noted that for relatively high input current (it depending on size and structure of the Omnimagnet), Solenoid 3 heats very rapidly, and the safe operating temperature is achieved quickly. For these power levels, heat dissipation by convective cooling is overwhelmed by the input power and changes in h are inconsequential.

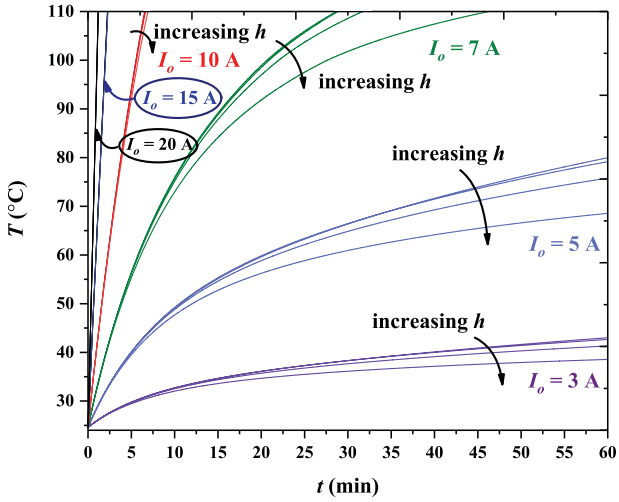

Fig. 6 The effect of heat transfer coefficient on the outer solenoid transient temperature (only solenoid on) at six different input currents (3, 5, 7, 10, 15, and 20 A). Arrows indicate increasing *h* (5, 250, 500, and 1000 (W/m^2·K)).

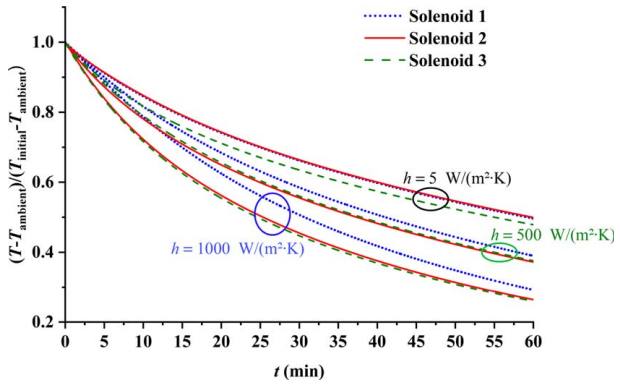

Fig. 7 The effect of heat transfer coefficient on the temperature of the three solenoids with no input current. The arrow indicates increasing *h* (5, 250, 500, and 1000 (W/m^2·K)).

It can be concluded that for high I, forced convection from the outer surfaces of the Omnimagnet by itself is not a suitable method to slow the heating process and to prevent undesirable effects of high temperature.

While convective cooling of the Omnimagnet is found to be insufficient for extending the operational time at relatively high input power, convective cooling should be effective when none of the solenoids is powered and the objective is to cool the entire device to an acceptable temperature level. To study the validity of this hypothesis, the transient response of non-dimensional temperature of the three solenoids is considered with no power applied to the device (Fig. 7). To calculate the initial temperature, it is assumed that all solenoids are powered for 60 min with $I = 3$ A. The temperature at the last time-step is used as the initial temperature of the cooling period. Initial temperatures for Solenoids 1, 2, and 3 are 75.3 °C, 71.1 °C, and 66.0 °C, respectively. A non-dimensional temperature is chosen to display the temporal response as the trends are self-similar for different initial temperatures. As expected, cooling rates are greater for increasing values of h. This is especially true for forced convection with air or a liquid. As expected, the outer solenoid (Solenoid 3) with its entire outer surface exposed to the convective environment cools at the highest rate. The data in Fig. 7 indicate that the cooling rate on the inner solenoid (Solenoid 1) is lower than the other two. The inner solenoid does not have direct contact with the ambient air, while the middle solenoid (Solenoid 2) has less surface area exposed to convection in comparison to the outer solenoid (Solenoid 3). While the cooling process is reasonably effective, it would be advantageous to find other means to reduce T_{max}, increase t_{max}, and decrease the cooling time to achieve a desired temperature level.

Conclusion

Thermal performance of an Omnimagnet is studied using a lumped capacitance model, which is validated with experimental data from a single Omnimagnet. An optimized model, which includes correction coefficients for the Omnimagnet used in the validation, is found to be in good agreement with the experimental data. The maximum root mean square error of the model is approximately 4% (data are normalized by temperature in degree celsius). Based on a parametric study that considers all seven possible combinations of powered solenoids, the safe range of input current, where the maximum temperature of the system does not reach the minimum critical temperature of the Omnimagnet components, is calculated. Increases to the external heat transfer coefficient are found to be beneficial only at low input current. With no power applied to the device, external convection is found to be much more beneficial for heat dissipation although cooling time is still significant.

Given the ineffectiveness of external convection, active cooling of device components, such as the frame or the interior sphere, should be considered to improve overall thermal performance of the Omnimagnet. The thermal model is linearized and presented as a state-space equation that can be applied in a Kalman filter controller. This model may be used as a basic thermal management tool for any type of omnidirectional electromagnetic device.

Acknowledgment

Research reported in this publication was supported by the National Institute on Deafness and Other Communication Disorders of the National Institutes of Health under Award Number R01DC013168. The content is solely the responsibility of the authors and does not necessarily represent the official views of the National Institutes of Health. We would like express our gratitude to Dr. Lisandro Leon for his assistance with the experiments. We also acknowledge the Center for High Performance Computing at the University of Utah for their support and resources, and in particular thank Dr. Martin Cuma for his assistance parallelizing the optimization code.

Conflicts of Interest

There are no conflicts of interest.

Data Availability Statement

The authors attest that all data for this study are included in the paper. The data that support the findings of this study are available from the corresponding author, upon reasonable request.

Appendix A: A Case Study

The implementation of the lumped-capacitance transient model on the Omnimagnet used for the validation experiments is presented in this section. The Omnimagnet consists of 16 components as indicated by the volume of each in Table 1. The components include the three solenoids, four frames, wire insulation on each solenoid (3), cover insulation on each solenoid (3), the air trapped within the inner solenoid by the middle solenoid (inner air), the spherical core, and the electric insulation paper between Solenoid 2 and Frame 4. Thin insulating paper is placed between all solenoids

and their adjacent frames; however, their impact on heat transfer in negligible with one exception. The insulating paper between Frame 4 and Solenoid 2 is included, because it transmits radiation to the ambient. Applying Eq. (1) to all 16 elements produces a set of 16 ODE equations with 16 unknown temperatures, which are solved at each time-step. The input data for the model are presented in Tables 1–7. Table 2 contains the constant thermal properties for the materials in each component. While the exact composition of the wire insulation is unknown, it consists primarily of polyamide. The specific heat capacity at constant pressure c_{pc} (Eq. (A1) [27–29]) and thermal conductivity κ_c (Eq. (A2) [27–29]) of copper are modeled as functions of temperature.

Volume data for each component are presented in Table 1. The volumes of the frames and core are extracted from SOLIDWORKS

Table 1 Component volume

Variable	Element	V (cm^3)	Number	Element	V (cm^3)
V_1	Solenoid 1 (Copper 1)	326	V_9	Cover insulation 1 (Solenoid 1)	4.2
V_2	Solenoid 2 (Copper 2)	285	V_{10}	Wire insulation 2 (Solenoid 2)	47.6
V_3	Solenoid 3 (Copper 3)	320	V_{11}	Cover insulation 2 (Solenoid 2)	5.5
V_4	Frame 1	2×27.77	V_{12}	Wire insulation 3 (Solenoid 3)	52.4
V_5	Frame 2	2×31.95	V_{13}	Cover insulation 3 (Solenoid 3)	6.9
V_6	Frame 3	2×25.46	V_{14}	Inside air	294
V_7	Frame 4	2×46.18	V_{15}	Spherical core	525
V_8	Wire insulation 1 (Solenoid 1)	54.9	V_{16}	Insulating paper	2.9

Table 2 Thermal properties for component materials

Component	$c_p\left(\frac{\text{kJ}}{\text{kg}\cdot\text{K}}\right)$	$\rho\left(\frac{\text{kg}}{\text{m}^3}\right)$	$k\left(\frac{\text{W}}{\text{m}\cdot\text{K}}\right)$	ϵ
Frame (aluminum)	0.896 [27]	2700 [27]	210 [27]	0.03 [27]
Wire (copper)	Eq. (A1) [27–29]	8960 [27]	Eq. (A2) [27–29]	0.78 (heated) [32]
Wire insulation (polyamide)	1.670 [33]	1140 [33]	0.25 [33]	0.6 [34]
Ferromagnetic core	0.502 [35]	8165.57 [35]	13 [35]	–
Cover insulation (polyurethane)	1.800 [36]	1200 [36]	0.024 [36]	0.9[37]
Inside trapped air	1.007 [27]	1.614 [27]	0.0263 [27]	–
Insulating paper	1.336 [27]	950 [27]	0.143 [27]	0.95 [27]

Table 3 Contact surface area

$S_{i,j,m}$	Element	$m=1$ x direction (cm^2)	$m=2$ y direction (cm^2)	$m=3$ z direction (cm^2)
$S_{1,8,m}$	Solenoid 1 + Wire insulation 1	112	179	177
$S_{1,9,m}$	Solenoid 1 + Cover insulation 1	0	228	232
$S_{2,10,m}$	Solenoid 2 + Wire insulation 2	266	38	294
$S_{2,11,m}$	Solenoid 2 + Cover insulation 2	326	0	285
$S_{3,12,m}$	Solenoid 3 + Wire insulation 3	381	362	72
$S_{3,13,m}$	Solenoid 3 + Cover insulation 3	422	403	0
$S_{4,5,m}$	Frame 1 + Frame 2	8	0	0
$S_{4,8,m}$	Frame 1 + Wire insulation 1	0	95	20
$S_{4,14,m}$	Frame 1 + Trapped inside air	11	90	12
$S_{4,15,m}$	Frame 1 + Sphere	0	17	0
$S_{5,6,m}$	Frame 2 + Frame 3	5	0	0
$S_{5,8,m}$	Frame 2 + Wire insulation 1	47	0	0
$S_{5,10,m}$	Frame 2 + Wire insulation 2	138	0	14
$S_{5,12,m}$	Frame 2 + Wire insulation 3	0	3.6	0
$S_{5,14,m}$	Frame 2 + Trapped inside air	65	27	43
$S_{6,0,m}$	Frame 3 + Ambient air	43	157	29.3
$S_{6,7,m}$	Frame 3 + Frame 4	0	6	0
$S_{6,10,m}$	Frame 3 + Wire insulation 2	0	5.4	0
$S_{6,12,m}$	Frame 3 + Wire insulation 3	15	155	0
$S_{7,0,m}$	Frame 4 + Ambient air	6	36	172
$S_{7,12,m}$	Frame 4 + Wire insulation 3	0	0	9
$S_{7,16,m}$	Frame 4 + Paper	0	0	43
$S_{8,14,m}$	Wire insulation 1 + Trapped inside air	0	90	151
$S_{9,0,m}$	Cover insulation 1 + Ambient air (middle channel)	0	134	0
$S_{9,10,m}$	Cover insulation 1+ Wire insulation 2	0	0	177
$S_{10,14,m}$	Wire insulation 2 + Inside air	72	0	220
$S_{11,0,m}$	Cover insulation 2 + Ambient air	0	0	160
$S_{11,12,m}$	Cover insulation 2 + Wire insulation 3	242	0	0
$S_{11,16,m}$	Cover insulation 2 + Paper	0	0	180
$S_{12,0,m}$	Wire insulation 3 + Ambient air (middle channel)	0	178	0
$S_{13,0,m}$	Cover insulation 3 + Ambient air	436	577	36
$S_{15,14,m}$	Sphere + Inside air	73	73	73
$S_{16,0,m}$	Paper + Ambient air	0	0	160

Table 4 Component thickness

$\Delta x_{j,m}$	$m = 1$ x-direction (cm)	$m = 2$ y-direction (cm)	$m = 3$ z-direction (cm)	$\Delta x_{j,m}$	$m = 1$ x-direction (cm)	$m = 2$ y-direction (cm)	$m = 3$ z-direction (cm)
$\Delta x_{1,m}$	10	1.4	1.4	$\Delta x_{2,m}$	0.8	11.9	0.8
$\Delta x_{3,m}$	0.7	12.1	0.7	$\Delta x_{4,m}$	10	0.6	2
$\Delta x_{5,m}$	0.5	12.7	1.1	$\Delta x_{6,m}$	1.1	0.3	1.2
$\Delta x_{7,m}$	1.2	14.3	0.6	$\Delta x_{8,m}$	0.6	0.08	0.08
$\Delta x_{9,m}$	10.06	0.02	0.02	$\Delta x_{10,m}$	0.05	0.7	0.05
$\Delta x_{11,m}$	0.02	12.11	0.02	$\Delta x_{12,m}$	0.04	0.04	0.8
$\Delta x_{13,m}$	0.02	0.02	13.67	$\Delta x_{14,m}$	0	0	0
$\Delta x_{15,m}$	4.5	3.7	4.5	$\Delta x_{16,m}$	10.06	7.51	0.01

Table 5 Convection coefficients

$h_{i,j}$	Nusselt number correlation	Characteristic length (m)	i	Reference
$(h_{i,14})_v$	$\overline{Nu}_L = 0.18\left(\frac{Pr}{0.2+Pr}Ra_L\right)^{0.29}$	$L = y_i - y_j$	4, 5, 8, 10, 15	[38]
$(h_{i,0})_{encl}$	$\overline{Nu}_L = \left[0.825 + \frac{0.387Ra_L^{1/6}}{[1+(0.492/Pr)^{9/16}]^{8/27}}\right]^2$	$L = L_i$	6, 7, 9, 12, 13	[39]
$(h_{i,0})_{hb}$	$\overline{Nu}_L = 0.52Ra_L{}^{1/5}$	$L = A_s/P$	11, 16	[40]
$(h_{i,0})_{ha}$	$\overline{Nu}_L = 0.54Ra_L{}^{1/4}$	$L = A_s/P$	11, 16	[41]

Table 6 Correction coefficients

$CF_{i,j,m}$	Component 1	Component 2	m	Value
$CF_{4,8,2}$	Frame 1	Wire insulation 1	Conduction (y direction)	0.41
$CF_{4,8,3}$	Frame 1	Wire insulation 1	Conduction (z direction)	0.33
$CF_{4,15,2}$	Frame 1	Sphere	Conduction (y direction)	0.04
$CF_{5,6,1}$	Frame 2	Frame 3	Conduction (x direction)	0.88
$CF_{5,8,1}$	Frame 2	Wire insulation 1	Conduction (x direction)	0.88
$CF_{5,10,1}$	Frame 2	Wire insulation 2	Conduction (x direction)	0.13
$CF_{5,10,3}$	Frame 2	Wire insulation 2	Conduction (z direction)	0.30
$CF_{5,12,3}$	Frame 2	Wire insulation 3	Conduction (y direction)	0.60
$CF_{6,7,2}$	Frame 3	Frame 4	Conduction (y direction)	0.03
$CF_{6,10,2}$	Frame 3	Wire insulation 2	Conduction (y direction)	0.95
$CF_{6,12,1}$	Frame 3	Wire insulation 3	Conduction (x direction)	0.05
$CF_{6,12,2}$	Frame 3	Wire insulation 3	Conduction (y direction)	0.18

CAD files. The volume of the solenoids, insulation layers, and the trapped air can be calculated using expressions provided in Ref. [1].

$$c_{pc} = 316.21 + 0.3177\,T_c - 3.5 \times 10^{-4}\,T_c^2 \quad \text{(A1)}$$

$$\kappa_c = 420.75 - 0.068493T_c \quad \text{(A2)}$$

The electrical resistance of wire is also modeled as a function of temperature (Eq. (A3)):

$$R = R_0(1 + \alpha_0(T - 293.15)) \quad \text{(A3)}$$

where R_0 is the initial electrical resistance of the wire, which is 3.2 Ω, 2.8 Ω, and 3.1 Ω for Solenoids 1, 2, and 3, respectively. The constant α_0 for copper is 0.0039 (1/K) [30,31].

Calculating the contact surface area between two adjacent components (Table 3) is time consuming and prone to uncertainty. In addition, the contact surface area depends on the Cartesian direction, as conduction is a vector quantity. Thus, in addition to the contact surface area, component thickness is determined for all three directions, as shown in Table 4. The thickness of one layer of wire insulation, which is defined as $\Delta x_{17,m}$, is 0.004 cm. The thickness of wire insulation between frame 4 and wire insulation 3 is considered to be equal to the thickness of the wire insulation.

Natural convection heat transfer coefficients are based on empirical correlations as presented in Table 5. The locations where they are applied are as follows: (1) between the inside trapped air and adjacent components, (2) between ambient air and Solenoid 3, (3) between ambient and the lower surface of Solenoid 2, and (4) between ambient and the upper surface of Solenoid 2.

$\overline{Nu}_L = h_{i,j}L/\kappa_i$, $\mathrm{Pr} = \nu/\alpha$, and $\mathrm{Ra}_L = g\beta(T_s - T_\infty)L^3/\nu\alpha$ represent average Nusselt number, Prandtl number, and Rayleigh number, respectively. ν is the kinematic viscosity (m^2/s), α is the thermal diffusivity (m^2/s), g is the gravity (m/s^2), β is the thermal expansion coefficient (1/K), and L is the characteristic length (m). The subscript "s" represents the surface and subscript "∞" represents ambient. A_s is the surface area of the hot surface (m^2), and P is the perimeter of the hot surface (m).

The melting temperature of the insulation covering the outside of each solenoid is 120 °C, which is the lowest of critical temperature of all the materials in the entire system. Therefore, this temperature determined the upper limit for the experiments. All heating experiments were terminated when the insulation achieved a temperature

Table 7 Correction coefficients for convection coefficients

$CF_{i,j}$	i	Component 2	Value
$(CF_{i,14})_v$	4, 5, 8, 10, 15	Inside trapped air	1.96
$(CF_{i,0})_{encl}$	6, 7, 9, 12, 13	Ambient air	2.74
$(CF_{i,0})_{ha,hb}$	11, 16	Ambient air	2.88

of 115 °C or after a total time of 2 h, whichever occurred first. As a result, the maximum time that the Omnimagnet was powered depends on input current; higher input current leads to shorter safe operating time. Experimental data acquired from this process were used to validate simulation results. Initially, the differences in solenoid temperatures between the experiment and simulations was as high as 25°C; however, the transient trends were similar. The maximum temperature difference was found to occur at the upper operational limits near 115 °C.

To reduce the error, and to ultimately create a more accurate model, 15 coefficients were added to the basic code. These correction coefficients were applied to the terms with uncertain dimensions (e.g., thickness, contact area) and where there was a high probability that contact resistance may be present. In addition, three correction coefficients were added to the convection terms to account for the uncertainty in convection heat transfer coefficients.

An optimization process was performed to determine appropriate values for the coefficients based on minimization of the solenoid temperature differences between experiments and simulations. During the optimization process, transient solenoid temperatures for seven experiments, corresponding to the seven combinations of powered solenoids, were evaluated and compared to simulation data determined under similar conditions. The MATLAB optimization toolbox (using the fmincon interior point algorithm [26]) was applied by varying the 15 coefficients using a quasi-Newton method.

The optimized correction coefficients were then applied to the terms shown in Tables 6 and 7. For this specific model, $CF_{i,j,m} = CF_{j,i,m}$. For the conduction correction coefficients, smaller values suggest conduction between components is insignificant, whereas values close to unity indicate more dominant conduction processes. Convection term correction coefficients suggest the heat transfer coefficients were underestimated by the correlations listed in Table 5.

Appendix B: State-Space Equations

A state-space equation may be used to predict the transient temperature through the entire Omnimagnet given a set of solenoid current values that may also vary with time. The predictions may be compared with the corresponding temperatures recorded from a limited number of thermocouples embedded within the device. By applying the Kalman filter, the error of prediction at each instance is reduced and temperatures at all points are calculated more precisely. An accurate prediction of temperature is desired to avoid increasing the temperature of any component above its melting point. Adjusting the current to avoid that scenario can be accomplished in real time using a feedback loop that includes temperature prediction. To this aim, the state-space equation of an Omnimagnet is presented as Eq. (B1):

$$\dot{\vec{T}} = A\vec{T} + B\vec{U} + GT_0 \tag{B1}$$

where $\dot{\vec{T}}$ is a set of n temperature derivatives with respect to time (for the Omnimagnet in Appendix A, $n = 16$), A is an $n \times n$ matrix, B is an $n \times 3$ matrix, and G is an $n \times 1$ matrix. $\vec{T}$ is a vector consisting of n temperatures, and $\vec{U}$ is the input vector consisting of the square of three input currents (I^2). The non-zero components of the A, B, and G matrices are listed here, in a general form and for the specific Omnimagnet presented in Appendix A. The round parenthesis are used when a parameter is function of temperature and brackets are used for grouping terms. The general form of matrix A components are defined by Eqs. (B2) and (B3):

$$A_{i,j} = \frac{1}{\rho_i c_{pi} V_i}\left[\sum_{j=1, j\neq i}^{j=n}\left(\sum_{m=1}^{m=3}\frac{\kappa_j S_{i,j,m}}{\Delta x_{j,m}}\right) + \left(\sum_{j=0|j=14}\sum_{m=1}^{m=3} h_{i,j} S_{i,j,m}\right) + \left(\sum_{m=1}^{m=3}\sigma\epsilon_i S_{i,0,m} T_i^3\right)\right] \tag{B2}$$

$$A_{i,i} = -\sum_{j=1, j\neq i}^{j=n} A_{i,j} \tag{B3}$$

The matrix A non-zero components for the Omnimagnet discussed in Appendix A are

$$A_{1,1} = -[A_{1,8} + A_{1,9}], \quad A_{1,8} = \frac{\kappa_8\left[\frac{S_{1,8,x}}{\Delta x_8} + \frac{S_{1,8,y}}{\Delta y_8} + \frac{S_{1,8,z}}{\Delta z_8}\right]}{\rho_1 c_{p1}(T_1) V_1}, \quad A_{1,9} = \frac{\kappa_9\left[\frac{S_{1,9,x}}{\Delta x_9} + \frac{S_{1,9,y}}{\Delta y_9} + \frac{S_{1,9,z}}{\Delta z_9}\right]}{\rho_1 c_{p1}(T_1) V_1}$$

$$A_{2,2} = -[A_{2,10} + A_{2,11}], \quad A_{2,10} = \frac{\kappa_{10}\left[\frac{S_{2,10,x}}{\Delta x_{10}} + \frac{S_{2,10,y}}{\Delta y_{10}} + \frac{S_{2,10,z}}{\Delta z_{10}}\right]}{\rho_2 c_{p2}(T_2) V_2}$$

$$A_{2,11} = \frac{-\kappa_{11}\left[\frac{S_{2,11,x}}{\Delta x_{11}} + \frac{S_{2,11,y}}{\Delta y_{11}} + \frac{S_{2,11,z}}{\Delta z_{11}}\right]}{\rho_2 c_{p2}(T_2) V_2}$$

$$A_{3,3} = -\left[A_{3,12} + A_{3,13} + \frac{\sigma\epsilon_3[S_{13,0,x} + S_{13,0,y} + S_{13,0,z}]T_3^3}{\rho_3 c_{p3}(T_3) V_3}\right], \quad A_{3,12} = \frac{\kappa_{12}\left[\frac{S_{3,12,x}}{\Delta x_{12}} + \frac{S_{3,12,y}}{\Delta y_{12}} + \frac{S_{3,12,z}}{\Delta z_{12}}\right]}{\rho_3 c_{p3}(T_3) V_3}$$

$$A_{3,13} = \frac{\kappa_{13}\left[\frac{S_{3,13,x}}{\Delta x_{13}} + \frac{S_{3,13,y}}{\Delta y_{13}} + \frac{S_{3,13,z}}{\Delta z_{13}}\right]}{\rho_3 c_{p3}(T_3) V_3}, \quad A_{4,4} = -\left[A_{4,5} + A_{4,8} + A_{4,14} + A_{4,15}\right]$$

$$A_{4,5}=\frac{\kappa_5\left[\frac{S_{4,5,x}}{\Delta x_5}+\frac{S_{4,5,y}}{\Delta y_5}+\frac{S_{4,5,z}}{\Delta z_5}\right]}{\rho_4 c_{p4} V_4},\quad A_{4,8}=\frac{\kappa_8\left[\frac{S_{4,8,x}}{\Delta x_8}+CF_{4,8,2}\frac{S_{4,8,y}}{\Delta y_8}+CF_{4,8,3}\frac{S_{4,8,z}}{\Delta z_8}\right]}{\rho_4 c_{p4} V_4}$$

$$A_{4,14}=\frac{(CF_{4,14}h_{4,14})_v\left[S_{4,14,x}+S_{4,14,y}+S_{4,14,z}\right]}{\rho_4 c_{p4} V_4},\quad A_{4,15}=\frac{\kappa_{15}\left[\frac{S_{4,15,x}}{\Delta x_{15}}+CF_{4,15,2}\frac{S_{4,15,y}}{\Delta y_{15}}+\frac{S_{4,15,z}}{\Delta z_{15}}\right]}{\rho_4 c_{p4} V_4}$$

$$A_{5,4}=\frac{\kappa_4\left[\frac{S_{4,5,x}}{\Delta x_4}+\frac{S_{4,5,y}}{\Delta y_4}+\frac{S_{4,5,z}}{\Delta z_4}\right]}{\rho_5 c_{p5} V_5},\quad A_{5,5}=-[A_{5,4}+A_{5,6}+A_{5,8}+A_{5,10}+A_{5,12}+A_{5,14}]$$

$$A_{5,6}=\frac{\kappa_6\left[CF_{5,6,1}\frac{S_{5,6,x}}{\Delta x_6}+\frac{S_{5,6,y}}{\Delta y_6}+\frac{S_{5,6,z}}{\Delta z_6}\right]}{\rho_5 c_{p5} V_5},\quad A_{5,8}=\frac{\kappa_8\left[CF_{5,8,1}\frac{S_{5,8,x}}{\Delta x_8}+\frac{S_{5,8,y}}{\Delta y_8}+\frac{S_{5,8,z}}{\Delta z_8}\right]}{\rho_5 c_{p5} V_5}$$

$$A_{5,10}=\frac{\kappa_{10}\left[CF_{5,10,1}\frac{S_{5,10,x}}{\Delta x_{10}}+\frac{S_{5,10,y}}{\Delta y_{10}}+CF_{5,10,3}\frac{S_{5,10,z}}{\Delta z_{10}}\right]}{\rho_5 c_{p5} V_5},\quad A_{5,12}=\frac{\kappa_{12}\left[\frac{S_{5,12,x}}{\Delta x_{12}}+\frac{S_{5,12,y}}{\Delta y_{12}}+CF_{5,12,3}\frac{S_{5,12,z}}{\Delta z_{12}}\right]}{\rho_5 c_{p5} V_5}$$

$$A_{5,14}=\frac{-(CF_{5,14}h_{5,14})_v[S_{5,14,1}+S_{5,14,2}+S_{5,14,3}]}{\rho_5 c_{p5} V_5}$$

$$A_{6,5}=\frac{\kappa_5\left[CF_{5,6,1}\frac{S_{5,6,x}}{\Delta x_5}+CF_{5,6,2}\frac{S_{5,6,y}}{\Delta y_5}+\frac{S_{5,6,z}}{\Delta z_5}\right]}{\rho_6 c_{p6} V_6}$$

$$A_{6,6}=-\left[A_{6,5}+A_{6,7}+A_{6,10}+A_{6,12}+\frac{(CF_{6,0}h_{6,0})_{encl}\left[S_{6,0,x}+S_{6,0,y}+S_{6,0,z}\right]}{\rho_6 c_{p6} V_6}\right]$$

$$A_{6,7}=\frac{\kappa_7\left[\frac{S_{6,7,x}}{\Delta x_7}+\frac{S_{6,7,y}}{\Delta y_7}+\frac{S_{6,7,z}}{\Delta z_7}\right]}{\rho_6 c_{p6} V_6},\quad A_{6,10}=\frac{\kappa_{10}\left[\frac{S_{6,10,x}}{\Delta x_{10}}+CF_{6,10,2}\frac{S_{6,10,y}}{\Delta y_{10}}+\frac{S_{6,10,z}}{\Delta z_{10}}\right]}{\rho_6 c_{p6} V_6},$$

$$A_{6,12}=\frac{\kappa_{12}\left[CF_{6,12,1}\frac{S_{6,12,x}}{\Delta x_{12}}+CF_{6,12,2}\frac{S_{6,12,y}}{\Delta y_{12}}+\frac{S_{6,12,z}}{\Delta z_{12}}\right]}{\rho_6 c_{p6} V_6},\quad A_{7,6}=\frac{\kappa_6\left[\frac{S_{6,7,x}}{\Delta x_6}+CF_{6,7,2}\frac{S_{6,7,y}}{\Delta y_6}+\frac{S_{6,7,z}}{\Delta z_6}\right]}{\rho_7 c_{p7} V_7}$$

$$A_{7,7}=-\left[A_{7,6}+A_{7,12}+A_{7,16}+\frac{-(CF_{7,0}h_{7,0})_{encl}\left[S_{7,0,x}+S_{7,0,y}+S_{7,0,z}\right]+\sigma\epsilon_7\left[S_{7,0,x}+S_{7,0,y}+S_{7,0,z}\right]T_7^3}{\rho_7 c_{p7} V_7}\right]$$

$$A_{7,12}=\frac{\kappa_{12}\left[\frac{S_{7,12,x}}{\Delta x_{17}}+\frac{S_{7,12,y}}{\Delta y_{17}}+\frac{S_{7,12,z}}{\Delta z_{17}}\right]}{\rho_7 c_{p7} V_7},\quad A_{7,16}=\frac{\kappa_{16}\left[\frac{S_{7,16,x}}{\Delta x_{16}}+\frac{S_{7,16,y}}{\Delta y_{16}}+\frac{S_{7,16,z}}{\Delta z_{16}}\right]}{\rho_7 c_{p7} V_7}$$

$$A_{8,1}=\frac{\kappa_1(T_1)\left[\frac{S_{1,8,x}}{\Delta x_1}+\frac{S_{1,8,y}}{\Delta y_1}+\frac{S_{1,8,z}}{\Delta z_1}\right]}{\rho_8 c_{p8} V_8},\quad A_{8,4}=\frac{\kappa_4\left[\frac{S_{4,8,x}}{\Delta x_4}+CF_{4,8,2}\frac{S_{4,8,y}}{\Delta y_4}+CF_{4,8,3}\frac{S_{4,8,z}}{\Delta z_4}\right]}{\rho_8 c_{p8} V_8}$$

$$A_{8,5}=\frac{\kappa_5\left[CF_{5,8,1}\frac{S_{5,8,x}}{\Delta x_5}+\frac{S_{5,8,y}}{\Delta y_5}+\frac{S_{5,8,z}}{\Delta z_5}\right]}{\rho_8 c_{p8} V_8},\quad A_{8,8}=-\left[A_{8,1}+A_{8,4}+A_{8,5}+A_{8,14}\right]$$

$$A_{8,14}=\frac{(CF_{8,14}h_{8,14})_v\left[S_{8,14,x}+S_{8,14,y}+S_{8,14,z}\right]}{\rho_8 c_{p8} V_8},\quad A_{9,1}=\frac{\kappa_1(T_1)\left[\frac{S_{1,9,x}}{\Delta x_1}+\frac{S_{1,9,y}}{\Delta y_1}+\frac{S_{1,9,z}}{\Delta z_1}\right]}{\rho_9 c_{p9} V_9}$$

$$A_{9,9}=-\left[A_{9,1}+A_{9,10}+\frac{(CF_{9,0}h_{9,0})_{encl}\left[S_{9,0,x}+S_{9,0,y}+S_{9,0,z}\right]}{\rho_9 c_{p9} V_9}\right],\quad A_{9,10}=\frac{\kappa_{10}\left[\frac{S_{9,10,x}}{\Delta x_{10}}+\frac{S_{9,10,y}}{\Delta y_{10}}+\frac{S_{9,10,z}}{\Delta z_{10}}\right]}{\rho_9 c_{p9} V_9}$$

$$A_{10,2}=\frac{\kappa_2(T_2)\left[\frac{S_{2,10,x}}{\Delta x_2}+\frac{S_{2,10,y}}{\Delta y_2}+\frac{S_{2,10,z}}{\Delta z_2}\right]}{\rho_{10} c_{p10} V_{10}},\quad A_{10,5}=\frac{\kappa_5\left[CF_{5,10,1}\frac{S_{5,10,x}}{\Delta x_5}+\frac{S_{5,10,y}}{\Delta y_5}+CF_{5,10,3}\frac{S_{5,10,z}}{\Delta z_5}\right]}{\rho_{10} c_{p10} V_{10}}$$

$$A_{10,6}=\frac{\kappa_6\left[\frac{S_{6,10,x}}{\Delta x_6}+CF_{6,10,2}\frac{S_{6,10,y}}{\Delta y_6}+\frac{S_{6,10,z}}{\Delta z_6}\right]}{\rho_{10} c_{p10} V_{10}},\quad A_{10,9}=\frac{\kappa_9\left[\frac{S_{9,10,x}}{\Delta x_9}+\frac{S_{9,10,y}}{\Delta y_9}+\frac{S_{9,10,z}}{\Delta z_9}\right]}{\rho_{10} c_{p10} V_{10}}$$

$$A_{10,10} = -\left[A_{10,2} + A_{10,5} + A_{10,6} + A_{10,9} + A_{10,14}\right]$$

$$A_{10,14} = \frac{(CF_{10,14}h_{10,14})_v\left[S_{10,14,x} + S_{10,14,y} + S_{10,14,z}\right]}{\rho_{10}c_{p10}V_{10}}, \quad A_{11,2} = \frac{\kappa_2(T_2)\left[\frac{S_{2,11,x}}{\Delta x_2} + \frac{S_{2,11,y}}{\Delta y_2} + \frac{S_{2,11,z}}{\Delta z_2}\right]}{\rho_{11}c_{p11}V_{11}}$$

$$A_{11,11} = -\left[A_{11,2} + A_{11,12} + A_{11,16} + \frac{(CF_{11,0})_{ha,hb}((h_{11,0})_{hb} + (h_{11,0})_{ha})S_{11,0,y}}{\rho_{11}c_{p11}V_{11}}\right]$$

$$A_{11,12} = \frac{\kappa_{12}\left[\frac{S_{11,12,x}}{\Delta x_{12}} + \frac{S_{11,12,y}}{\Delta y_{12}} + \frac{S_{11,12,z}}{\Delta z_{12}}\right]}{\rho_{11}c_{p11}V_{11}}, \quad A_{11,16} = \frac{\kappa_{16}\left[\frac{S_{11,16,x}}{\Delta x_{16}} + \frac{S_{11,16,y}}{\Delta y_{16}} + \frac{S_{11,16,z}}{\Delta z_{16}}\right]}{\rho_{11}c_{p11}V_{11}}$$

$$A_{12,3} = \frac{\kappa_3(T_3)\left[\frac{S_{3,12,x}}{\Delta x_3} + \frac{S_{3,12,y}}{\Delta y_3} + \frac{S_{3,12,z}}{\Delta z_3}\right]}{\rho_{12}c_{p12}V_{12}}, \quad A_{12,5} = \frac{\kappa_5\left[\frac{S_{5,12,x}}{\Delta x_5} + \frac{S_{5,12,y}}{\Delta y_5} + CF_{5,12,3}\frac{S_{5,12,z}}{\Delta z_5}\right]}{\rho_{12}c_{p12}V_{12}}$$

$$A_{12,6} = \frac{\kappa_6\left[CF_{6,12,1}\frac{S_{6,12,x}}{\Delta x_6} + CF_{6,12,2}\frac{S_{6,12,y}}{\Delta y_6} + \frac{S_{6,12,z}}{\Delta z_6}\right]}{\rho_{12}c_{p12}V_{12}}, \quad A_{12,7} = \frac{\kappa_7\left[\frac{S_{7,12,x}}{\Delta x_7} + \frac{S_{7,12,y}}{\Delta y_7} + \frac{S_{7,12,z}}{\Delta z_7}\right]}{\rho_{12}c_{p12}V_{12}}$$

$$A_{12,11} = \frac{\kappa_{11}\left[\frac{S_{11,12,x}}{\Delta x_{11}} + \frac{S_{11,12,y}}{\Delta y_{11}} + \frac{S_{11,12,z}}{\Delta z_{11}}\right]}{\rho_{12}c_{p12}V_{12}}$$

$$A_{12,12} = -[A_{12,3} + A_{12,5} + A_{12,6} + A_{12,7} + A_{12,11} + \cdots,$$
$$\cdots \frac{\sigma\epsilon_{12}\left[S_{12,0,x} + S_{12,0,y} + S_{12,0,z}\right]T_{12}^3 + (CF_{12,0}h_{12,0})_{encl}\left[S_{12,0,x} + S_{12,0,y} + S_{12,0,z}\right]}{\rho_{12}c_{p12}V_{12}}]$$

$$A_{13,3} = \frac{\kappa_3(T_3)\left[\frac{S_{3,13,x}}{\Delta x_3} + \frac{S_{3,13,y}}{\Delta y_3} + \frac{S_{3,13,z}}{\Delta z_3}\right]}{\rho_{13}c_{p13}V_{13}}$$

$$A_{13,13} = A_{13,3} + \frac{(CF_{13,0}h_{13,0})_{encl}\left[S_{13,0,x} + S_{13,0,y} + S_{13,0,z}\right] + \sigma\epsilon_{13}\left[S_{13,0,x} + S_{13,0,y} + S_{13,0,z}\right]T_{13}^3}{\rho_{13}c_{p13}V_{13}}$$

$$A_{14,4} = \frac{(CF_{4,14}h_{4,14})_v\left[S_{4,14,x} + S_{4,14,y} + S_{4,14,z}\right]}{\rho_{14}c_{p14}V_{14}}, \quad A_{14,5} = \frac{(CF_{5,14}h_{5,14})_v\left[S_{5,14,x} + S_{5,14,y} + S_{5,14,z}\right]}{\rho_{14}c_{p14}V_{14}}$$

$$A_{14,8} = \frac{(CF_{8,14}h_{8,14})_v\left[S_{8,14,x} + S_{8,14,y} + S_{8,14,z}\right]}{\rho_{14}c_{p14}V_{14}}, \quad A_{14,10} = \frac{(CF_{10,14}h_{10,14})_v\left[S_{10,14,x} + S_{10,14,y} + S_{10,14,z}\right]}{\rho_{14}c_{p14}V_{14}}$$

$$A_{14,14} = -\left[A_{14,4} + A_{14,5} + A_{14,8} + A_{14,10} + A_{14,15}\right]$$

$$A_{14,15} = \frac{(CF_{15,14}h_{15,14})_v\left[S_{14,15,x} + S_{14,15,y} + S_{14,15,z}\right]}{\rho_{14}c_{p14}V_{14}}$$

$$A_{15,4} = \frac{\kappa_4\left[\frac{S_{4,15,x}}{\Delta x_4} + CF_{4,15,2}\frac{S_{4,15,y}}{\Delta y_4} + \frac{S_{4,15,z}}{\Delta z_4}\right]}{\rho_{15}c_{p15}V_{15}}, \quad A_{15,14} = \frac{(CF_{15,14}h_{15,14})_v\left[S_{14,15,x} + S_{14,15,y} + S_{14,15,z}\right]}{\rho_{15}c_{p15}V_{15}}$$

$$A_{15,15} = -\left[A_{15,4} + A_{15,14}\right], \quad A_{16,7} = \frac{\kappa_7\left[\frac{S_{7,16,x}}{\Delta x_7} + \frac{S_{7,16,y}}{\Delta y_7} + \frac{S_{7,16,z}}{\Delta z_7}\right]}{\rho_{16}c_{p16}V_{16}}$$

$$A_{16,11} = \frac{\kappa_{11}\left[\frac{S_{11,16,x}}{\Delta x_{11}} + \frac{S_{11,16,y}}{\Delta y_{11}} + \frac{S_{11,16,z}}{\Delta z_{11}}\right]}{\rho_{16}c_{p16}V_{16}}$$

$$A_{16,16} = -\left[A_{16,7} + A_{16,11} + \cdots \frac{(CF_{16,0})_{ha,hb}((h_{16,0})_{hb} + (h_{16,0})_{ha})\left[S_{16,0,x} + S_{16,0,y} + S_{16,0,z}\right] + \sigma\epsilon_{16}\left[S_{16,0,x} + S_{16,0,y} + S_{16,0,z}\right]T_{16}^3}{\rho_{16}c_{p16}V_{16}}\right]$$

B is an $n \times 3$ matrix. The general form of the components of B is (Eq. (B4))

$$B_{i,j} = \frac{R_i}{\rho_i c_{pi} V_i} \tag{B4}$$

where the non-zero components represent the contribution of the electrical current.

For the Omnimagnet in Appendix A, B is a 16×3 matrix and the non-zero components are

$$B_{1,1}=\frac{R(T_1)}{\rho_1 c_{p1}(T_1)V_1},\quad B_{2,2}=\frac{R(T_2)}{\rho_2 c_{p2}(T_2)V_2},\quad B_{3,3}=\frac{R(T_3)}{\rho_3 c_{p3}(T_3)V_3} \tag{B5}$$

G is a $n\times1$ matrix in general and the components are expressed as (Eq. (B6))

$$G_{i,0}=\frac{1}{\rho_i c_{pi} V_i}\left[\left(\sum_{m=1}^{m=3} h_{i,0}S_{i,0,m}\right)+\left(\sum_{m=1}^{m=3}\sigma\epsilon_i S_{i,0,m}T_0^3\right)\right] \tag{B6}$$

For the Omnimagnet in Appendix A, G is a 16×1 matrix with the following nonzero components:

$$G_{3,0}=\frac{\sigma\epsilon_3\left[S_{13,0,x}+S_{13,0,y}+S_{13,0,z}\right]T_0^3}{\rho_3 c_{p3}(T_3)V_3},\quad G_{6,0}=\frac{(CF_{6,0}h_{6,0})_{encl}\left[S_{6,0,x}+S_{6,0,y}+S_{6,0,z}\right]}{\rho_6 c_{p6}V_6}$$

$$G_{7,0}=\frac{(CF_{7,0}h_{7,0})_{encl}\left[S_{7,0,x}+S_{7,0,y}+S_{7,0,z}\right]+\sigma\epsilon_7\left[S_{7,0,x}+S_{7,0,y}+S_{7,0,z}\right]T_0^3}{\rho_7 c_{p7}V_7}$$

$$G_{9,0}=\frac{(CF_{9,0}h_{9,0})_{encl}\left[S_{9,0,x}+S_{9,0,y}+S_{9,0,z}\right]}{\rho_9 c_{p9}V_9},\quad G_{11,0}=\frac{(CF_{11,0})_{ha,hb}((h_{11,0})_{ha}+(h_{11,0})_{hb})S_{11,0,y}}{\rho_{11}c_{p11}V_{11}}$$

$$G_{12,0}=\frac{(CF_{12,0}h_{12,0})_{encl}\left[S_{12,0,x}+S_{12,0,y}+S_{12,0,z}\right]+\sigma\epsilon_{12}\left[S_{12,0,x}+S_{12,0,y}+S_{12,0,z}\right]T_0^3}{\rho_{12}c_{p12}V_{12}}$$

$$G_{13,0}=\frac{(CF_{13,0}h_{13,0})_{encl}\left[S_{13,0,x}+S_{13,0,y}+S_{13,0,z}\right]+\sigma\epsilon_{13}(\left[S_{13,0,x}+S_{13,0,y}+S_{13,0,z}\right]T_0^3}{\rho_{13}c_{p13}V_{13}}$$

$$G_{16,0}=\frac{(CF_{16,0})_{ha,hb}((h_{16,0})_{ha}+(h_{16,0})_{hb})\left[S_{16,0,x}+S_{16,0,y}+S_{16,0,z}\right]+\sigma\epsilon_{16}\left[S_{16,0,x}+S_{16,0,y}+S_{16,0,z}\right]T_0^3}{\rho_{16}c_{p16}V_{16}}$$

References

[1] Petruska, A. J., and Abbott, J. J., 2014, "Omnimagnet: An Omnidirectional Electromagnet for Controlled Dipole-Field Generation," IEEE. Trans. Magn., **50**(7), pp. 1–10.

[2] Petruska, A. J., Mahoney, A. W., and Abbott, J. J., 2014, "Remote Manipulation With a Stationary Computer-Controlled Magnetic Dipole Source," IEEE Transactions on Robotics, **30**(5), pp. 1222–1227.

[3] Clark, J. R., Leon, L., Warren, F. M., and Abbott, J. J., 2012, "Magnetic Guidance of Cochlear Implants: Proof-of-Concept and Initial Feasibility Study," ASME J. Med. Dev., **6**(3), p. 035002–8.

[4] Leon, L., Warren, F. M., and Abbott, J. J., 2018, "An in-vitro Insertion-Force Study of Magnetically Guided Lateral-Wall Cochlear-implant Electrode Arrays," Otology Neur., **39**(2), pp. e63–e73.

[5] Leon, L., Warren, F. M., and Abbott, J. J., 2018, "Optimizing the Magnetic Dipole-Field Source for Magnetically Guided Cochlear-Implant Electrode-Array Insertions," J. Med. Robot. Res., **3**(1), pp. 1–37.

[6] Campelo, H. M. R., Quintela, M. A., Torriano, F., Labbé, P., and Picher, P., 2016, "Numerical Thermofluid Analysis of a Power Transformer Disc-Type Winding," 2016 IEEE Electrical Insulation Conference (EIC), Montreal, QC, Canada, June 19–22, IEEE, pp. 362–365.

[7] Mufuta, J. M., 2000, "Modelling of the Mixed Convection in the Windings of a Disc-Type Power Transformer," Appl. Therm. Eng., **20**(5), pp. 417–437.

[8] Tsili, M. A., Amoiralis, E. I., Kladas, A. G., and Souflaris, A. T., 2012, "Power Transformer Thermal Analysis by Using An Advanced Coupled 3D Heat Transfer and Fluid Flow Fem Model," Int. J. Therm. Sci., **53**(1), pp. 188–201.

[9] Allahbakhshi, M., and Akbari, M., 2016, "Heat Analysis of the Power Transformer Bushings Using the Finite Element Method," Appl. Therm. Eng., **100**(May), pp. 714–720.

[10] Campelo, H., Lopez-Fernandez, X. M., Picher, P., and Torriano, F., 2013, "Advanced Thermal Modelling Techniques in Power Transformers. Review and Case Studies," Advanced Research Workshop on Transformers, Baiona, Spain, pp. 6–21.

[11] Coddé, J., der Veken, W. V., and Baelmans, M., 2015, "Assessment of a Hydraulic Network Model for Zig-Zag Cooled Power Transformer Windings," Appl. Therm. Eng., **80**, pp. 220–228.

[12] Rodriguez, G. R., Garelli, L., Storti, M., Granata, D., Amadei, M., and Rossetti, M., 2017, "Numerical and Experimental Thermo-Fluid Dynamic Analysis of a Power Transformer Working in Onan Mode," Appl. Therm. Eng., **112**(February), pp. 1271–1280.

[13] Torriano, F., Chaaban, M., and Picher, P., 2010, "Numerical Study of Parameters Affecting the Temperature Distribution in a Disc-Type Transformer Winding," Appl. Therm. Eng., **30**(14), pp. 2034–2044.

[14] Torriano, F., Campelo, H., Quintela, M., Labbé, P., and Picher, P., 2018, "Numerical and Experimental Thermofluid Investigation of Different Disc-Type Power Transformer Winding Arrangements," Int. J. Heat Fluid Flow, **69**(1), pp. 62–72.

[15] Contreras, J., Rodriguez, E., and Taha-Tijerina, J., 2017, "Nanotechnology Applications for Electrical Transformers—A Review," Electric Power Syst. Res., **143**(Feb.), pp. 573–584.

[16] Fontes, D. H., Ribatski, G., and Filho, E. P. B., 2015, "Experimental Evaluation of Thermal Conductivity, Viscosity and Breakdown Voltage ACc of Nanofluids of Carbon Nanotubes and Diamond in Transformer Oil," Diamond. Relat. Mater., **58**(September), pp. 115–121.

[17] Guan, W., Jin, M., Fan, Y., Chen, J., Xin, P., Li, Y., Dai, K., Zhang, H., Huang, T., and Ruan, J., 2014, "Finite Element Modeling of Heat Transfer in a Nanofluid Filled Transformer," IEEE. Trans. Magn., **50**(2), pp. 253–256.

[18] Modestov, M., Kolemen, E., Fisher, A., and Hvasta, M., 2017, "Electromagnetic Control of Heat Transport Within a Rectangular Channel Filled With Flowing Liquid Metal," Nucl. Fusion., **58**(1), p. 016009–9.

[19] Patel, J., Parekh, K., and Upadhyay, R., 2016, "Prevention of Hot Spot Temperature in a Distribution Transformer Using Magnetic Fluid As a Coolant," Int. J. Therm. Sci., **103**(May), pp. 35–40.

[20] Weinberg, M., and Senyurt, A., 2017, "Polyamide Electrical Insulation for Use in Liquid Filled Transformers," Patent No: WO2017123948A1, USA, https://patents.google.com/patent/WO2017123948A1/en.

[21] Lekawa–Raus, A., Patmore, J., Kurzepa, L., Bulmer, J., and Koziol, K., 2014, "Electrical Properties of Carbon Nanotube Based Fibers and Their Future Use in Electrical Wiring," Adv. Funct. Mater., **24**(24), pp. 3661–3682.

[22] Esmailie, F., Cavilla, M. S., and Ameel, T. A., 2017, "A Thermal Transient Model of Heat Transfer Within an Omnimagnet," ASME 2017 International Mechanical Engineering Congress and Exposition, Tampa, FL, Nov. 3–9, ASME, p. V008T10A046–10.

[23] Shampine, L., and Reichelt, M., 1997, "The Matlab Ode Suite," SIAM J. Sci. Comput., **18**(1), pp. 1–22.

[24] Fluke, *Fluke 83 V and 87 V Digital Multimeters Detailed Specifications*.

[25] Fluke, *USB-TEMP and USB-TC Series, Temperature Measurement Devices*.

[26] Kiusalaas, J., 2015, *Numerical Methods in Engineering With MATLAB®*, 3rd ed., Cambridge University Press, New York.

[27] Incropera, F. P., DeWitt, D. P., Lavine, A. S., and Bergman, T. L., 2011, *Fundamentals of Heat and Mass Transfer*, 7th ed., Wiley, Hoboken, NJ.

[28] Pure Copper, https://www.engineersedge.com/properties_of_metals.htm, Last accessed July 2020.

[29] Haynes, W. M., Lide, D. R., and Thomas, J. B., 2016, *Handbook of Chemistry and Physics: A Ready-Reference Book of Chemical and Physical Data*, CRC Press, Boca Raton, Florida.

[30] Temperature Coefficient of Copper, https://www.cirris.com/learning-center/general-testing/special-topics/177-temperature-coefficient-of-copper, Last accessed July 2020.
[31] Dellinger, J. H., 1970, *Bulletin of the Bureau of Standards*, U.S. G.P.O, Washington.
[32] Engineering ToolBox, 2003, "Emissivity Coefficients Materials," https://www.engineeringtoolbox.com/emissivity-coefficients-d_447.html, Last accessed July 2020.
[33] Polyamide - nylon 6 (pa 6), http://www.goodfellow.com/E/Polyamide-Nylon-6.html, Last accessed July 2020.
[34] Xiao, T., Fan, X., Fan, D., and Li, Q., 2017, "High Thermal Conductivity and Low Absorptivity/ Emissivity Properties of Transparent Fluorinated Polyimide Films," Polym. Bull., **74**(1), pp. 4561–4575.
[35] EFI alloy 50 (aka magnifer 502, carpenter high permeability 491, alloy 47–50). https://www.edfagan.com/index.php/soft-magnetic-alloys/alloy-50/alloy-50-properties/, Last accessed July 2020.
[36] Polyurethane Insulation-Engineering Toolbox, https://www.engineeringtoolbox.com/polyurethane-insulation-k-values-d˙1174.html, Last accessed July 2020.
[37] Martinez, I., "Properties of Solids," http://webserver.dmt.upm.es/~isidoro/dat1/eSol.pdf, Last accessed October 2020.
[38] Catton, I., 1978, "Natural Convection in Enclosures," 6th International Heat Transfer Conference, Toronto, Canada, Aug. 7–11, pp. 13–31.
[39] Churchill, S. W., and Chu, H. H., 1975, "Correlating Equations for Laminar and Turbulent Free Convection From a Vertical Plate," Int. J. Heat. Mass. Transfer., **18**(11), pp. 1323–1329.
[40] Radziemska, E., and Lewandowski, W., 2001, "Heat Transfer by Natural Convection From An Isothermal Downward-Facing Round Plate in Unlimited Space," Appl. Energy., **68**(4), pp. 347–366.
[41] Lloyd, J. R., and Moran, W. R., 1974, "Natural Convection Adjacent to Horizontal Surface of Various Planforms," ASME J. Heat. Transfer., **96**(4), pp. 443–447.